Mon. Not. R. Astron. Soc. **000**, 1–?? (2004) Printed 2 February 2008 (MN LATEX style file v2.2)

Evidence for X-ray Obscuration in Type II Quasar Candidates from the Sloan Digital Sky Survey

Cristian Vignali,[1,2⋆] Dave M. Alexander[3⋆] and Andrea Comastri[1⋆]

[1] *INAF – Osservatorio Astronomico di Bologna, Via Ranzani 1, 40127 Bologna, Italy*
[2] *Dipartimento di Astronomia, Università degli Studi di Bologna, Via Ranzani 1, 40127 Bologna, Italy*
[3] *Institute of Astronomy, Madingley Road, Cambridge, CB3 0HA*

arXiv:astro-ph/0407293v1 14 Jul 2004

Accepted 2004 ???. Received 2004 ???; in original form 2004 ???

ABSTRACT

Recently, Zakamska et al. (2003) selected 291 high-ionization narrow emission-line AGN in the redshift range 0.3–0.83 from the Sloan Digital Sky Survey spectroscopic data. The sample includes both Seyfert II galaxies and their higher luminosity "cousins", Type II quasar candidates. Here we present the results on the X-ray properties of 17 of these objects for which archival X-ray data (*ROSAT* and XMM-*Newton*) are available. Three sources have been significantly ($\gtrsim 6\sigma$) detected, one being the most radio-loud source of the sample; its X-ray emission, possibly enhanced by jet emission, is consistent with the absence of absorption. Another source has a $\approx 6\sigma$ detection in the *ROSAT* All-Sky Survey, possibly complex radio structure, and no evidence for strong X-ray absorption. For the third X-ray detection, the XMM-*Newton* spectrum indicates a column density of $N_{\rm H} = 1.26^{+0.75}_{-0.51} \times 10^{22}$ cm^{-2}; this result, coupled with the 2–10 keV luminosity of $\approx 4 \times 10^{44}$ erg s^{-1}, makes this source a genuine Type II quasar. Using the [O III]λ5007 line luminosities, we estimated the intrinsic X-ray power of the AGN and found that $\gtrsim 47$ per cent of the observed sample shows indications of X-ray absorption, with column densities $\gtrsim 10^{22}$ cm^{-2}. This provides further evidence that a considerable fraction are obscured quasars. Support to our conclusions also comes from the recent analysis of RASS data performed by Zakamska et al. (2004), who found five additional lower significance ($\approx 2.1\sigma - 3.6\sigma$) X-ray matches.

Key words: galaxies: active — galaxies: nuclei — quasars: general — X-rays

1 INTRODUCTION

One of the basic predictions of Unification models of active galactic nuclei (AGN) is the existence of a population of luminous, highly obscured (i.e., with high-ionization, narrow optical emission-line spectra) AGN, the so-called Type II quasars, often referred to as the higher luminosity counterparts of local Seyfert II galaxies. In the X-ray band these objects are expected to be highly luminous ($\gtrsim$ a few $\times 10^{44}$ erg s^{-1}) and absorbed by column densities $\gtrsim 10^{22}$ cm^{-2}; given their properties, they would constitute an important ingredient of most AGN synthesis models for the X-ray background (XRB; e.g., Comastri et al. 2001; Gilli, Salvati & Hasinger 2001). Before the advent of the current generation of X-ray telescopes (*Chandra* and XMM-*Newton*), Type II quasars formed quite an elusive class of sources [but see Brandt et al. (1997) and Franceschini et al. (2000)]. Recent X-ray surveys have found several genuine Type II quasars (e.g., Norman et al. 2002; Stern et al. 2002; Fiore et al. 2003; Perola et al. 2004; Gandhi et al. 2004; Caccianiga et al. 2004; Szokoly et al. 2004) and many more candidate Type II quasars (e.g., Crawford et al. 2001, 2002; Mainieri et al. 2002; Barger et al. 2003). Multiwavelength observations of these objects generally support their Type II quasar status; in particular, at optical wavelengths Type II quasars often show high equivalent width, narrow emission lines with high-ionization line ratios. However, in some cases broad-band, high signal-to-noise ratio optical/near-infrared follow-up observations of X-ray selected Type II quasar candidates have revealed broad components in their permitted emission lines (e.g., Halpern et al. 1999; Akiyama et al. 2002). Overall, less than ≈ 20 per cent of the hard X-ray, presumably absorbed sources found in moderately deep/ultra-deep surveys have optical counterparts characterized by high-ionization narrow emission lines (e.g., Barger et al. 2003), suggesting that the Type II quasar population is not adequately sampled at present. Furthermore, the optical counterparts of X-ray selected Type II quasar candidates are typically so faint that the spectroscopic identification is quite a challenging task. Therefore, to have a comprehensive view

⋆ E-mail: cristian.vignali@bo.astro.it (CV); dma@ast.cam.ac.uk (DMA); andrea.comastri@bo.astro.it (AC).

© 2004 RAS

of the properties of Type II quasars, the selection of a relatively optically bright sample is necessary. In this regard, recently Zakamska et al. (2003; hereafter Z03) selected 291 high-ionization narrow emission line AGN in the redshift range 0.3–0.83 from the Sloan Digital Sky Survey (SDSS; York et al. 2000) spectroscopic data. The sample includes both Seyfert II galaxies and their higher luminosity "cousins", Type II quasar candidates. This is the only published optically selected sample of candidate Type II quasars in this redshift range.[1] The main goal of the present work is to define the basic X-ray properties of optically selected Type II quasar candidates.

Hereafter we adopt the "concordance" (WMAP) cosmology (H_0=70 km s^{-1} Mpc^{-1}, $\Omega_{\rm M}$=0.3, and Ω_Λ=0.7; Spergel et al. 2003).

2 SAMPLE SELECTION

To select candidate obscured (i.e., Type II) AGN from the SDSS spectroscopic data, Z03 searched for objects with narrow emission lines without underlying broad components and with line ratios characteristic of non-stellar ionizing radiation. The redshift range (0.3–0.83) is chosen to include the [O III]λ5007 line in all of the spectra and this allows a statistically relevant study of the emission-line properties of the sources. The sample members are characterized by spectra with signal-to-noise ratios $\geqslant 7.5$, rest-frame equivalent width of the [O III] line $\geqslant 4$ Å, and FWHM (Hβ) < 2000 km s^{-1}. The high-ionization selection criteria adopted by Z03 (see § 3.3 of Z03 and Kewley et al. 2001 for further references) are designed to properly reject star-forming galaxies and genuinely unobscured objects, such as narrow-line Seyfert 1 galaxies (NLS1s), which otherwise would match the FWHM criterion (e.g., Williams, Pogge & Mathur 2002). Given the width of the fibers used in the SDSS spectroscopic runs (3″), a significant contribution to the overall emission can come from the AGN host galaxies. To compute reliable AGN emission-line parameters, Z03 subtracted the host galaxy contribution from each spectrum (using templates) before computing the line parameters. About 50 per cent of the objects selected by Z03 have [O III] line luminosities in the range $3\times10^8 - 10^{10}$ $L_\odot$, comparable to those of luminous ($-27 < M_{\rm B} < -23$) quasars. This, coupled with other evidences, suggests that at least the objects in the luminous subsample are Type II quasar candidates.[2]

It must be noted that Z03 sample, is not complete; $\approx$ 28 per cent of the sources have been selected as "targets", $\approx$ 42 per cent as "serendipitous", $\approx$ 19 per cent from the Deep Southern Equatorial Scan (DSES) plates (where the magnitude limit is $\approx$ 1 mag fainter), and 11 per cent from the "special plates" (see Z03 for details). Nevertheless, the careful and accurate analyses performed by Z03 to select the final sample of 291 candidate obscured AGN allow reliable studies of optically selected Type II quasar candidates.

3 THE X-RAY DATA: REDUCTION AND ANALYSIS

The Z03 catalog of candidate Type II quasars was cross correlated with archival *ROSAT*, *Chandra*, and XMM-*Newton* observations. Our basic X-ray source searching strategy is performed using *ROSAT* because of its large field-of-view. On the contrary, *Chandra* and XMM-*Newton* cover smaller regions of the sky but provide greater sensitivity and broader energy range (up to $\approx$ 10 keV). Seventeen sources lie in archival X-ray observations. The observation log and source X-ray fluxes (or upper limits) are presented in Table 1.

3.1 ROSAT observations

At first the Z03 sample was cross correlated with *ROSAT* data [pointed PSPC, pointed HRI, and the *ROSAT* All-Sky Survey (RASS)]. We used only the central regions (20′ radius) of the *ROSAT* PSPC and HRI detectors, where the sensitivity is highest and the PSPC window support structure does not affect source detection. This maximizes the probability of detecting faint sources. In cases of multiple observations of the same SDSS quasar with the same X-ray instrument, the one with the best combination of off-axis angle and exposure time has been chosen. Typically, the use of PSPC data is preferred to that of HRI data, given the larger number of objects with PSPC data available.[3] The detailed source detection procedure is described in Vignali, Brandt & Schneider (2003). Briefly, source detection was performed in the 0.5–2 keV band for the PSPC and in the full band ($\approx$ 0.1–2.4 keV) for the HRI. A conservative matching radius of 40″ was used to take into account the broadening of the Point Spread Function (PSF) at large off-axis angles,[4] although typically a good match is obtained within 15–20″ (e.g., Vignali et al. 2003).

Standard likelihood detection algorithms available under MIDAS/EXSAS (Zimmermann et al. 1998) have been used. We set the detection threshold to a likelihood of $L = -\ln(P_{\rm e}) = 6$, corresponding to a probability $P_{\rm e}$ of the order of 2.5×10^{-3} that the observed number of photons in the source cell is produced entirely by a background fluctuation (corresponding to the $\approx 3.2\sigma$ detection level; Cruddace, Hasinger & Schmitt 1988).

Sixteen of the Z03 SDSS AGN fall in the inner part of the field-of-view of *ROSAT* pointed observations. Two have X-ray detections (one in the PSPC and the other in both the PSPC and HRI); these X-ray counterparts lie at 0.″1 (source #148) and 8.″2 (source #204) from the optical position; given their relatively large fluxes (see Table 1), we do not expect either of these sources to be spurious. We determined X-ray count rates (for the two detections) and 3σ upper limits for the 14 X-ray non-detections (12 from PSPC and 2 from HRI) using the SOSTA task in the XIMAGE package (version 4.1; Giommi et al. 1992). For the two X-ray detections the X-ray count rates obtained using XIMAGE have been compared with those derived using the maximum likelihood method, finding

[1] We note that Djorgovski et al. (2001) have produced a sample of obscured quasar candidates, selected on the basis of narrow permitted emission lines and high-ionization line ratios. This sample covers the complementary 0.31–0.36 redshift range.

[2] A widely accepted definition of Type II quasars does not exist at present. From the optical perspective, Type II quasars are the luminous [typically $M_{\rm B} < -23$ (e.g., Schmidt & Green 1983), although this "historical" absolute magnitude limit has not a physically supported motivation and is based on a different cosmology than the one adopted here] analogs of Seyfert II galaxies. In the X-rays, objects with 2–10 keV luminosity $\gtrsim 3\times10^{44}$ erg s^{-1} and characterized by absorption $\gtrsim 10^{22}$ cm^{-2} are usually called Type II quasars. We note that *a priori* it is possible that the objects optically classified as Type II quasars do not match the X-ray definition and viceversa. Therefore, in the following we will refer to our objects as Type II quasar candidates.

[3] For source #59 we report the results from both the PSPC and HRI observations.

[4] See ftp://ftp.xray.mpe.mpg.de/rosat/catalogues/1rxp/wga_rosatsrc.html.

Table 1. Zakamska et al. (2003) Type II AGN in *ROSAT* and XMM-*Newton* archival data.

Src[a] ID #	SDSS J	z	$N_{\rm H,gal}$[b] (10^{20} cm^{-2})	$S_{1.4\ \rm GHz}$[c] (mJy)	$\log L_{[O\ III]}$ ($L_\odot$)	$\log L_{2-10\ \rm keV}$[d]	Instr.[e]	$F_{0.5-2\ \rm keV}$[f]	Exp. Time (ks)	Off-axis Angle ($'$)	Obs.[g] ID
34	021047.01−100152.9	0.540	2.17	<0.48	9.79	45.1±0.6	P	<2.00	14.6	19.6	800114p
55	023359.93+004012.7	0.388	2.82	<0.42	8.17	43.5±0.6	P	<0.43	28.2	6.8	800482p
59	024309.79+000640.3	0.414	3.56	<0.84	7.95	43.3±0.6	P	<3.15	5.5	10.3	150021p−2
59[h]							H	<0.92	72.0	9.5	701352h−1
68	025558.00−005954.0	0.700	6.33	<0.42	8.51	43.9±0.6	P	<3.54	3.0	15.4	190338p
70	025951.28+002301.0	0.505	7.14	<0.42	8.53	43.9±0.6	P	<2.87	5.0	16.4	700393p
130	084234.94+362503.1	0.561	3.41	1.64	10.10	45.5±0.6	H	<2.53	28.1	5.7	800854h
148	090933.51+425346.5	0.670	1.60	4009.5	8.92	44.3±0.6	P	39.5	22.1	0.2	700329p−1
152	092014.11+453157.3	0.402	1.51	<2.13	9.04	44.4±0.6	P	<2.75	4.3	12.0	700539p
174	100854.43+461300.7	0.544	0.95	7.16	8.32	43.7±0.6	H	<3.42	9.5	17.5	702430h
188	104505.39+561118.4	0.428	0.65	2.59	9.08	44.4±0.6	P	<3.51	3.9	14.0	600058p
204	122656.48+013124.3	0.732	1.84	<2.22	9.66	45.0±0.6	P	2.63	24.8	12.5	600242p−1
204[i]						44.6–44.7	X	3.90	7.8–9.8	6.0	0110990201
208	123453.10+640510.2	0.594	1.87	<0.45	8.77	44.1±0.6	P	<4.74	3.0	17.0	800263p
209	124736.07+023110.7	0.487	1.76	0.90	8.59	43.9±0.6	P	<3.61	5.5	17.5	700020p
212	130740.56−021455.3	0.425	1.75	1.66	8.92	44.3±0.6	P	<8.37	1.6	18.2	200531p
239	150117.96+545518.3	0.338	1.40	20.87[j]	9.06	44.4±0.6	R	30.3	1.1		930725p
256	164131.73+385840.9	0.596	1.16	2.80	9.92	45.3±0.6	P	<2.44	5.5	16.1	201538p
258	165627.28+351401.7	0.679	1.73	1.16	8.57	43.9±0.6	P	<1.53	22.1	18.1	400374p

[a] From Table 1 of Zakamska et al. 2003. [b] From Dickey & Lockman 1990. [c] Integrated 1.4 GHz flux density (or 3σ upper limit) from FIRST (Becker, White & Helfand 1995). [d] Predicted 2–10 keV luminosity and relative uncertainty (using the 1σ scatter in the Mulchaey et al. 1994 correlation; see §4 for details) in units of erg s^{-1}. [e] "P" and "H" indicate the *ROSAT* PSPC and HRI observations, respectively, while "R" indicates the *ROSAT* All-Sky Survey (RASS) observation (in this case the off-axis angle is not reported); "X" is referred to the object with XMM-*Newton* observation. [f] Galactic absorption-corrected flux (or 3σ upper limit) in the observed 0.5–2 keV band, in units of 10^{-14} erg cm^{-2} s^{-1}. [g] Observation ID in the *ROSAT* (*ROSAT* observation request, ROR) and XMM-*Newton* archives. [h] Both PSPC and HRI data are reported for source #59, since the results obtained from their analyses appear significantly different (see text and Table 2 for details). [i] XMM-*Newton* observation of source #204. The flux and observed (de-absorbed) 2–10 keV luminosity shown here have been derived directly from X-ray spectral fitting of XMM-*Newton* data (see §4.1); the range is due to slight pn–MOS differences in relative normalisations. Both the pn and MOS exposure times after the removal of periods of flaring background are reported. [j] The flux density is referred to the FIRST source which is closest ($0.3''$) to the optical position of the quasar. This object has possibly a peculiar radio morphology, as reported in the Appendix A.4 and Fig. 2 of Zakamska et al. (2004).

good agreement. The X-ray count rates have been converted using PIMMS (Mukai 2001) into observed 0.5–2 keV fluxes (for both PSPC and HRI; this energy range corresponds to ≈ 0.7–3.5 keV in the source rest frame) using a power law with $\Gamma = 2.0$ and Galactic absorption (from Dickey & Lockman 1990). Although both Type I (i.e., with broad permitted emission lines) and Type II (i.e., with narrow permitted and forbidden emission lines) AGN in the local Universe are generally well described by Γ=1.8–2.0 X-ray continua (e.g., Nandra & Pounds 1994; Reeves & Turner 2000; Risaliti et al. 2002; Deluit & Courvoisier 2003; Malizia et al. 2003), it must be kept in mind that an additional soft X-ray component (perhaps related to the AGN host galaxy, to a circumnuclear starburst or to a scattering component; see, e.g., Vignali et al. 2001) could be present. However, the redshift range of the present sample partially reduces the contribution of this soft component to the measured 0.5–2 keV fluxes. For the sources where both the PSPC and HRI measurements are available, we compared the X-ray fluxes (upper limits). These are usually similar (but see Table 1 for the case of source #59), therefore we decided to use the PSPC measurements since they are available for the majority of the sources in the present sample. For the X-ray detected source #148, a variability of a factor of ≈ 2 over time-scales of ≈ 5 yr seems to be present. This is not surprising since X-ray variability over time-scales of several years are often observed in AGN (Almaini et al. 2000; Markowitz, Edelson & Vaughan 2003); furthermore, this source is also the most radio-loud AGN in Z03 sample (see Table 1), so enhanced variability, perhaps related to a jet component, might be present. Also in this case the PSPC measurement is used.

To match the Z03 sample with the RASS (Voges et al. 1999), we used the *ROSAT* Web Browse[5] assuming a matching radius of $40''$ and adopted a slightly more conservative detection threshold ($L = 8$, corresponding to the ≈ 3.7σ detection level) than that adopted for *ROSAT* pointed observations. One candidate Type II quasar is detected (at the ≈ 6σ level) in the RASS (source #239 in Table 1). The detection of this source in the RASS was possible due to a longer than typical exposure (≈ 1100 s as compared to typical values of ≈ a few hundred seconds for most of the other Z03 sources). The X-ray upper limits for the majority of the Z03 sources in the RASS are not sensitive enough for the purposes of this study.

Recently, Zakamska et al. (2004) have searched for the counterparts of their Type II AGN at radio/infrared wavelengths and in the X-ray band (using the RASS only). They found six sources with a counterpart in the RASS (at $0.31 < z < 0.61$) using a matching radius of $1'$ (see their Table 4). Among these, source #239 is in common with our list (see Table 1), while all of the remaining sources are below the detection threshold adopted in the present paper (three have $\lesssim 3.0\sigma$ detections, one is detected at the 3.4σ level, and one at the 3.6σ level). Two of these five matched sources have likely radio counterparts, thus increasing the reliability of their X-ray detection in the shallow RASS fields. However, the visual inspection of the individual RASS images provides evidence for weak X-ray emission only in the 3.4σ RASS source (having also a radio counterpart). Including the additional five lower significance (≈ 2.1σ − 3.6σ) RASS sources from Zakamska et al. (2004) would provide eight X-ray detections of Type II quasar candidates, although in the following we will refer only to the three higher significance X-ray sources matching our more conservative selec-

[5] See http://www.xray.mpe.mpg.de/cgi-bin/rosat/src-browser.

tion criteria. As pointed out by Zakamska et al. (2004), it is interesting to note that the fraction of SDSS Type I AGN (in the redshift range $0.3 < z < 0.8$) having RASS counterpart is significantly higher ($\approx$ 15-20 per cent) than that of Z03 SDSS Type II AGN. This can be explained assuming the presence of X-ray obscuration ($\approx 2 \times 10^{22}$ cm^{-2}, Zakamska et al. 2004); a similar result is clearly found in §4 of the present paper on a larger sample of Type II quasar candidates with deeper X-ray observations and also via direct X-ray spectral analysis (for source #204, see §4.1).

3.2 Chandra observations

Only one source in the Z03 sample [#130 (OBS_ID=532); also reported as HRI upper limit; see Table 1] lies within an archival *Chandra* observation (on-axis exposure time of $\approx$ 8.1 ks) but is not detected. Unfortunately, its position, very close to the edge of ACIS-I field-of-view, prevents a reliable determination of the source X-ray flux upper limit.

3.3 XMM-Newton observations

Two sources of the Z03 sample fall in XMM-*Newton* archival observations. One is a clear X-ray detection (source #204, also detected by *ROSAT* PSPC; see Table 1); the spectral analysis of this source using EPIC pn and MOS data is presented in §4.1. The XMM-*Newton* data were reduced with the version 5.4.1 of the Science Analysis Software (SAS) following the procedure described in Vignali et al. (2004). The data were filtered to avoid background flares which affect large intervals ($\approx$ 60–70 per cent) of our observation. The tasks EPPROC and EMPROC were used to generate valid photon list; patterns 0–4 and 0–12 were used for pn and MOS, respectively. Source counts were extracted in the 0.3–10 keV band from circular regions of radius $30''$ (pn) and $40''$ (MOS), while background counts were extracted from off-source regions of radius $90''$ (pn) and $80''$ (MOS). Response functions for spectral fitting were generated using the tasks RMFGEN and ARFGEN.

The other source [object #59 (OBS_ID=0111200101), also reported as PSPC upper limit; see Table 1] is not detected; its position, close to the edge of EPIC-pn field-of-view, does not allow us to derive a reliable X-ray flux upper limit, despite the long exposure of the observation ($\approx$ 37 ks).

3.4 Summary of X-ray observations

Overall, three sources of the Z03 sample have X-ray detections with *ROSAT* (sources #148, #204, and #239) assuming the matching criteria and detection thresholds reported in §3.1. Source #204, serendipitously found and detected also by XMM-*Newton*, has enough counts for a moderate-quality spectral analysis; the most relevant results are presented in §4.1.

4 CONSTRAINTS ON THE X-RAY PROPERTIES OF TYPE II QUASAR CANDIDATES

The distribution of the [O III] luminosities ($L_{[O\,III]}$) vs. redshift for the Z03 sources is shown in Fig. 1. Large open circles indicate the sources having X-ray upper limits, while the three large filled circles indicate the objects with X-ray detections. Most of the sources with X-ray information have [O III] line luminosities in the range $3\times10^8 - 10^{10}\ L_\odot$ (region above the dashed line in Fig. 1) which are comparable to those of luminous ($-27 < M_B < -23$)

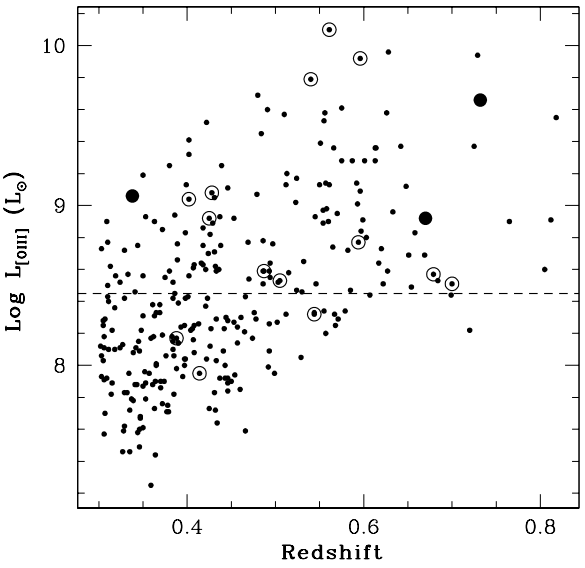

Figure 1. Logarithm of $L_{[O\,III]}$ luminosities vs. redshifts for all of the sources in Z03 catalog (small filled circles). The large open circles indicate the objects with X-ray upper limits, while the three X-ray detections are shown as large filled circles. Objects above the dashed line have [O III] line luminosities in the range $\approx 3\times10^8 - 10^{10}\ L_\odot$ which are comparable to those of luminous ($-27 < M_B < -23$) quasars; see Z03 for details.

quasars (Z03). In other words, *most of our X-ray observed objects are Type II quasar candidates* (see Footnote 2).

To derive basic constraints on the X-ray emission of Type II quasar candidates, we have used the correlation between the [O III] flux and the 2–10 keV flux found for Seyfert II galaxies (Mulchaey et al. 1994), adopting the parameterization reported in §3.2 of Collinge & Brandt (2000). Using this approach, we have computed the expected 2–10 keV flux for each source and, using the 1σ scatter in the correlation of Mulchaey et al. (1994), also the corresponding error range. It must be noted that no correction has been applied to the [OIII] line flux for the absorption due the narrow-line region itself [see Maiolino et al. (1998) and Bassani et al. (1999) for details]. This effect is usually corrected for by using the Balmer decrement, but unfortunately the spectral coverage of the Hα line is not available for most of the objects in the present sample. This approach leads to a conservative determination in whether or not a source is absorbed in the X-ray band.

The predicted 2–10 keV fluxes (with their 1σ uncertainties) have been converted into soft (0.5–2 keV) X-ray fluxes assuming a power law with photon index $\Gamma = 2$, which seems to be a relatively good parameterization for the intrinsic X-ray continuum of both Type I and Type II AGN (e.g., Nandra & Pounds 1994; Deluit & Courvoisier 2003).[6]

The soft X-ray fluxes derived following the method described above have then been compared with those observed (or the 3σ upper limits for the X-ray non-detections; see Table 1). This has allowed us to estimate on a source-by-source basis the amount of X-ray absorption required to match the derived soft X-ray flux with

[6] The assumption of $\Gamma = 1.9$ instead of 2.0 provides lower 0.5–2 keV fluxes (by $\approx$ 14 per cent).

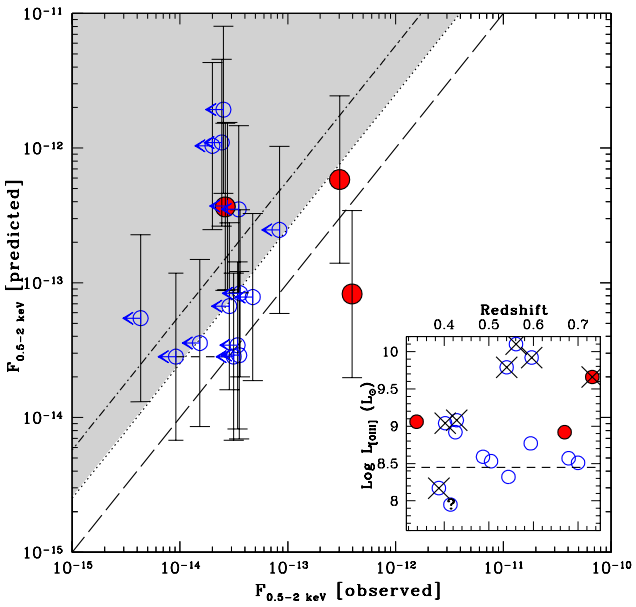

Figure 2. Predicted vs. observed soft X-ray flux for Z03 objects with archival X-ray observations. The filled circles indicate the three X-ray detections. Note the large X-ray flux for the right-most object (source #148) of the plot; this is also the most radio-loud source in the Z03 sample. The dashed diagonal line shows the 1:1 correlation, while the dotted (dot-dashed) line indicates the correlation expected for a source at $z = 0.5$ if the column density is 1×10^{22} cm^{-2} (3×10^{22} cm^{-2}). The horizontal dashed line connects the observed PSPC and HRI upper limits for source #59. The grey region shows the locus of likely absorbed ($N_{\rm H} > 10^{22}$ cm^{-2}) sources. The column densities associated with our objects, given the method used for their derivation, should be considered conservative (see §4 for details). In the inset, the $L_{[O\ III]}$ vs. redshift (as Fig. 1) is plotted for the objects with X-ray observations. The crosses indicate the likely absorbed objects (see Table 2); the "?" indicates source #59, where absorption is probably present only in the HRI observation (see text and Table 2).

the observed one. Since the derived soft X-ray flux has an associated scatter (due to that of the Mulchaey et al. 1994 correlation), for each source we determine an "allowed" range of column densities ($N_{\rm H,z}-$ and $N_{\rm H,z}+$ in Table 2). For sake of completeness, the column density range associated with each source is shown in Fig. 2. This procedure is based on *the simplest assumption made possible by the data at our disposal, i.e., these Type II quasar candidates have the same underlying average X-ray continuum of local Seyfert I galaxies and quasars, the only difference being the amount of X-ray absorption, which has been assumed to be intrinsic to the source.* Clearly, the uncertainties associated with the predicted soft X-ray fluxes (and thus with the derived column densities) are large. However, within our assumptions, these column densities (see Table 2) should be considered as lower limits, since all but three of our sources are not detected in the soft X-ray band.

At least 47 per cent (8/17) of the sources with X-ray information shows indications of X-ray absorption (see Fig. 2 and Table 2), with column densities typically $\gtrsim 10^{22}$ cm^{-2} (dotted line in Fig. 1 for a source at $z = 0.5$). A column density of ≈ 1–2×10^{22} cm^{-2}, close to the $N_{\rm H,z}-$ value, has been obtained also for source #204, whose X-ray properties have been derived via direct X-ray spectral analysis using XMM-*Newton* data (see §4.1 and Fig. 3).

We also tried to perform a stacking analysis combining all of the X-ray undetected sources. Although an $\approx 4\sigma$ detection has been

Table 2. Constraints on the X-ray column densities derived from *ROSAT* data.

Src ID #	Column Density[a]			X-ray[b] Det.	Likely[c] Abs.	QSO II[d]
	$N_{\rm H,z}$	$N_{\rm H,z}-$	$N_{\rm H,z}+$			
34	1.2×10^{23}	6.0×10^{22}	2.0×10^{23}		$\surd$	$*$
55	4.6×10^{22}	1.1×10^{22}	9.6×10^{22}		$\surd$	
59	0	0	1.5×10^{22}			
59[e]	1.2×10^{22}	7.0×10^{21}	4.9×10^{22}		$\surd$	
68	0	0	2.0×10^{22}			
70	8.0×10^{21}	0	4.7×10^{22}			
130	1.5×10^{23}	8.0×10^{22}	2.3×10^{23}		$\surd$	$*$
148	0	0	0	‡		
152	5.0×10^{22}	1.3×10^{22}	1.0×10^{23}		$\surd$	$*$
174	0	0	2.3×10^{22}			
188	4.3×10^{22}	8.5×10^{21}	9.5×10^{22}		$\surd$	$*$
204	8.7×10^{22}	2.3×10^{22}	1.8×10^{23}	‡	$\surd$	$*$
208	5.0×10^{21}	0	4.1×10^{22}			
209	9.0×10^{21}	0	4.6×10^{22}			
212	1.7×10^{22}	0	4.9×10^{22}			
239	4.7×10^{21}	0	3.0×10^{23}	‡		
256	1.3×10^{23}	6.0×10^{22}	2.1×10^{23}		$\surd$	$*$
258	1.2×10^{22}	0	6.2×10^{22}			

The column densities reported here (in cm^{-2}) should be considered as lower limits for all those objects which have not been detected by *ROSAT*. For the three X-ray detected sources, the column density range ($N_{\rm H,z}-$, $N_{\rm H,z}+$) is broadly consistent with the absorption derived by the hardness-ratio analysis.

[a] The three values of column densities have been obtained using the best-fitting value and the corresponding scatter in the Mulchaey et al. (1994) correlation between the [O III] flux and the 2–10 keV flux found for Seyfert II galaxies; this correlation has been applied to our data and used to estimate the expected 0.5–2 keV flux range for each object. Then the estimated 0.5–2 keV fluxes have been compared with the observed 0.5–2 keV fluxes (or 3σ upper limits) to derive $N_{\rm H,z}$, $N_{\rm H,z}-$, and $N_{\rm H,z}+$ on a source-by-source basis. Given the procedures adopted to derive the column densities (see §4 for details), $N_{\rm H,z}$ should be considered a conservative estimate. [b] ‡ means that the object is detected by *ROSAT*; see Table 1. [c] $\surd$ marks the sources which are likely absorbed (i.e., $N_{\rm H,z}- > 0$); see text for details. [d] $*$ indicates the possibly absorbed sources with X-ray luminosities $\gtrsim 3 \times 10^{44}$ erg s^{-1}(see Table 1 and Footnote 2). [e] For this source, HRI data indicate the presence of absorption. The time interval between the PSPC and HRI observations is ≈ 2 yr.

obtained, the total number of X-ray source counts (≈ 34) did not allow us to derive an average column density through hardness-ratio analysis. However, we compared the average flux derived from the stacking analysis (weighted by the exposure time of each observation with respect to the total) with that expected on the basis of the correlation of Mulchaey et al. (1994). An average column density of 1.4–2.7×10^{23} cm^2 has been derived, although we note that this value suffers from significant uncertainties. More reliable constraints could be obtained using *Chandra*, given the lower background and sharper PSF.

A caveat to the plain use of the method described above is related to the fact that the observations in the optical and X-ray bands are not simultaneous. Intrinsic source variability as well as variability in the absorbing medium over the time-scales probed by the X-ray observations might be present. However, our approach, although limited by the paucity of X-ray detections, is simple and designed to place basic constraints on the overall X-ray properties of optically selected, Type II quasar candidates.

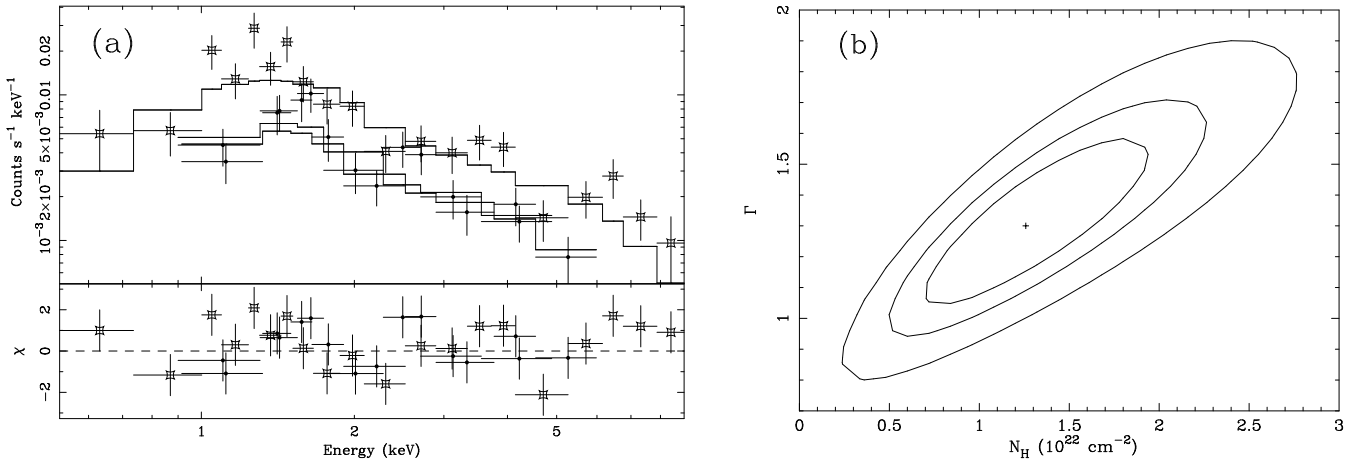

Figure 3. XMM-*Newton* data of source #204: (a) pn (larger symbols) +MOS1+MOS2 (small filled circles) spectral data (top panel) and data/model residuals (bottom panel, in units of σ); (b) 68, 90, and 99 per cent confidence contours for the photon index vs. intrinsic column density; see §4.1 for details.

4.1 X-ray spectral analysis of source #204: XMM-Newton results

Source #204 has ≈ 510 counts in the pn+MOS1+MOS2 data. These counts were grouped into spectra such that each spectral bin contained at least 15 counts to allow χ^2 fitting. X-ray spectra were fitted using the XSPEC package (version 11.2; Arnaud 1996). The quoted errors on the derived model parameters correspond to the 90 per cent confidence level for one interesting parameter (i.e., $\Delta\chi^2 = 2.71$; Avni 1976). All spectral fits include absorption due to the line-of-sight Galactic column density (from Dickey & Lockman 1990; see Table 1). Separate spectral fitting indicates that pn and MOS spectral results are consistent to within ≈ 10 per cent; this is similar to the value quoted by Kirsch (2003; ≈ 13 per cent). Therefore in the following the pn and MOS data will be fitted together with the same model leaving the relative normalisations free to vary.

A single power-law model is clearly not an adequate fit to XMM-*Newton* data; the quality of the fit is poor (χ^2/d.o.f.=61.2/32) and the photon index is very flat ($\Gamma = 0.74^{+0.12}_{-0.13}$), suggesting the presence of absorption. If an absorber at the source redshift ($z = 0.732$) is added to the previous model, the fit improves significantly (χ^2/d.o.f.=45.4/31), although some residuals are still present at energies around 1.5 keV. These can be partially accounted for by the addition of a thermal component (MEKAL model in XSPEC), perhaps related to the AGN host galaxy or to a circumnuclear starburst, but the spectral parameters of this component are poorly constrained, and therefore it will not be considered in the following. The best-fitting spectrum [shown in Fig. 3, panel (a)] is parameterized by a photon index $\Gamma = 1.30^{+0.16}_{-0.24}$ and a column density $N_{\rm H} = 1.26^{+0.75}_{-0.51} \times 10^{22}$ cm^{-2}. The 68, 90, and 99 per cent confidence contours for the photon index vs. column density are shown in Fig. 3 [panel (b)]. If the photon index is forced to be $\Gamma = 1.8 - 2.0$, more representative of the typical AGN intrinsic X-ray emission, the column density becomes 2.2–3.2×10^{22} cm^{-2}, more consistent with the $N_{\rm H}$ range derived from *ROSAT* data and reported in Table 2. We note, however, that source variability may have occurred between the *ROSAT* and XMM-*Newton* observations (over a time-scale of ≈ 10 yr). The intrinsic 2–10 keV luminosity ($10^{44.6-44.7}$ erg s^{-1}), the column density (≈ 1–2×10^{22} cm^{-2}), and the narrow-line optical spectrum (Z03) are fully consistent with source #204 being a genuine Type II quasar.

5 DISCUSSION

Though not complete, the catalog of Z03 provides an optically well-defined sample of candidate Type II quasars which can be used as a starting point for detailed analyses of the broad-band properties of optically luminous Type II quasars and for the study of the contribution of this population to the hard XRB (e.g., Gilli et al. 2001). In particular, Type II quasars might be crucial to study the dependence of absorption upon X-ray luminosity (Ueda et al. 2003; La Franca et al., in preparation). Since the sources of the present sample are mostly optically luminous, this study can be considered complementary to that of X-ray selected Type II quasar candidates, whose optical counterparts are typically faint and often hamper an accurate spectroscopic identification. Clearly, the results presented in this paper suffer from significant uncertainties, mostly related to the scatter in the correlation between the [O III] line intensity and hard X-ray flux (Mulchaey et al. 1994), the applicability of this method to the higher luminosity "cousins" of local Seyfert II galaxies (from which the correlation is obtained), and the assumption that all the AGN spectra have on average the same $\Gamma \approx 2$ underlying X-ray continuum. The first of these three major sources of uncertainty has been taken into account by comparing the observed soft X-ray fluxes and upper limits with those obtained using the correlation above. The uncertainties related to the scatter in the correlation (vertical error bars in Fig. 2) affect the derivation of the column densities (see the values $N_{\rm H,z}-$ and $N_{\rm H,z}+$ in Table 2); it must be kept in mind, however, that the predicted soft X-ray fluxes have been compared mostly with the observed X-ray flux upper limits, therefore the column densities should be treated as lower limits. Furthermore, intrinsically flatter X-ray slopes would produce lower column densities (by ≈ 20 per cent, if $\Gamma = 1.6$ instead of 2.0 is adopted), while the presence of an additional soft X-ray component (e.g., thermal emission from the host galaxy, scattering, etc.) would produce the opposite effect. Given the lack of spectral constraints provided by direct X-ray fitting (except for source #204), this approach, although a bit simplistic, allowed us to derive basic X-ray constraints for 17 Type II AGN, some of which being quasar candidates:

(i) At least 47 per cent of the present sample shows indications of X-ray absorption, with column densities $\gtrsim 10^{22}$ cm^{-2}.

(ii) The presence of genuine Type II quasars among the objects presented in this paper finds further support from the only object (source #204) with XMM-*Newton* moderate-quality spectral data

(§4.1). The intrinsic 2–10 keV luminosity ($\approx 10^{44.6}$ erg s^{-1}), the column density (≈ 1–2×10^{22} cm^{-2}), and the narrow-line optical spectrum of this source are consistent with the Type II quasar definition. Moreover, its X-ray luminosity is comparable with those of some higher redshift X-ray selected Type II quasars (e.g., Stern et al. 2002; Mainieri et al. 2002; Brusa et al. 2003).

Our results find further support from those obtained recently by Zakamska et al. (2004) on the basis of RASS data only.

The large-area surveyed by the SDSS, coupled with the relatively bright flux limit, the spectroscopic target selection and wavelength coverage, is such to possibly provide large numbers of optically selected Type II quasar candidates to be followed-up at other wavelengths with, e.g., *Spitzer*, *SCUBA* and current X-ray telescopes such as *Chandra* and XMM-*Newton*. Therefore, in the following years it will become possible to properly assess the broad-band properties of optically selected Type II quasars (in particular, their spectral energy distribution) and estimate their contribution to the hard XRB.

ACKNOWLEDGMENTS

CV and AC acknowledge partial support by the Italian Space agency under the contract ASI I/R/057/02. DMA is supported by the Royal Society. The authors would like to thank L. Angeretti for help with the plots, M. Mignoli and L. Pozzetti for useful discussions, and G. Zamorani for a careful reading of the manuscript. CV gratefully remembers Rosa B.

REFERENCES

Akiyama M., Ueda Y., Ohta, K., 2002, ApJ, 567, 42
Almaini O. et al., 2000, MNRAS, 315, 325
Arnaud K.A., 1996, in Jacoby G., Barnes J., eds, ASP Conf. Ser. Vol. 101, Astronomical Data Analysis Software and Systems V. Astron. Soc. Pac., San Francisco, p. 17
Avni Y., 1976, ApJ, 210, 642
Barger A.J. et al., 2003, AJ, 126, 632
Bassani L., Dadina M., Maiolino R., Salvati M., Risaliti G., della Ceca R., Matt G., Zamorani G., 1999, ApJS, 121, 473
Becker R.H., White R.L., Helfand D.J., 1995, ApJ, 450, 559
Brandt W.N., Fabian A.C., Takahashi K., Fujimoto R., Yamashita A., Inoue H., Ogasaka Y., 1997, MNRAS, 290, 617
Brusa M. et al., 2003, A&A, 409, 65
Caccianiga A. et al., 2004, A&A, 416, 901
Collinge M.J., Brandt W.N., 2000, MNRAS, 317, L35
Comastri A. et al., 2001, MNRAS, 327, 781
Crawford C.S., Fabian A.C., Gandhi P., Wilman R.J., Johnstone R.M., 2001, MNRAS, 324, 427
Crawford C.S., Gandhi P., Fabian A.C., Wilman R.J., Johnstone R.M., Barger A.J., Cowie L.L., 2002, MNRAS, 333, 809
Cruddace R.G., Hasinger G., Schmitt, J.H.M.M., 1988, in Murtagh F., Heck A., eds, ESO Conf. and Workshop Proc. 28, Astronomy from large databases: Scientific objectives and methodological approaches, p. 177
Deluit S., Courvoisier T.J.-L., 2003, A&A, 399, 77
Dickey J.M., Lockman F.J., 1990, ARA&A, 28, 215
Djorgovski S.G., Mahabal A.A., Brunner R.J., Gal R.R., Castro S., de Carvalho R.R., Odewahn S.C., 2001, in Brunner R.J., Djorgovski S.G., Szalay A.S., eds, ASP Conf. Ser. 225, Virtual Observatories of the Future. Astron. Soc. Pac., San Francisco, p. 52
Fiore F. et al., 2003, A&A, 409, 79
Franceschini A., Bassani L., Cappi M., Granato G.L., Malaguti G., Palazzi E., Persic M., 2000, A&A, 353, 910
Gandhi P., Crawford C.S., Fabian A.C., Johnstone R.M., 2004, MNRAS, 348, 529
Gilli R., Salvati M., Hasinger G., 2001, A&A, 366, 407
Giommi P., Angelini L., Jacobs P., Tagliaferri G., 1992, in Worrall D.M., Biemesderfer C., Barnes J., eds, ASP Conf. Ser. 25, Astronomical Data Analysis Software and Systems I. Astron. Soc. Pac., San Francisco, p. 100
Halpern J., Turner T., George I., 1999, MNRAS, 307, L47
Kewley L.J., Dopita M.A., Sutherland R.S., Heisler C.A., Trevena J., 2001, ApJ, 556, 121
Kirsch M., 2003, XMM-*Newton* Users Group Meeting Presentations (CAL-TN-0018-2-1)
Mainieri V. et al., 2002, A&A, 393, 425
Maiolino R., Salvati M., Bassani L., Dadina M., della Ceca R., Matt G., Risaliti G., Zamorani G., 1998, A&A, 338, 781
Malizia A., Bassani L., Stephen J.B., Di Cocco G., Fiore F., Dean A.J., 2003, ApJ, 589, L17
Markowitz A., Edelson R., Vaughan S., 2003, ApJ, 598, 935
Mukai K., 2001, PIMMS Users' Guide (Greenbelt: NASA/GSFC)
Mulchaey J.S. et al., 1994, ApJ, 436, 586
Nandra K., Pounds K.A., 1994, MNRAS, 268, 405
Norman C. et al., 2002, ApJ, 571, 218
Perola G.C. et al., 2004, A&A, 421, 491
Reeves J.N., Turner M.J.L., 2000, MNRAS, 316, 234
Risaliti G., 2002, A&A, 386, 379
Schmidt M., Green R.F., 1983, ApJ, 269, 352
Spergel D.N. et al., 2003, ApJS, 148, 175
Stern D. et al., 2002, ApJ, 568, 71
Szokoly G.P. et al., 2004, ApJS, in press (astro-ph/0312324)
Ueda Y., Akiyama M., Ohta K., Miyaji T., 2003, ApJ, 598, 886
Vignali, C., Comastri, A., Fiore, F., & La Franca, F. 2001, A&A, 370, 900
Vignali C., Brandt W.N., Schneider D.P., 2003, AJ, 125, 433
Vignali C., Brandt W.N., Boller Th., Fabian A.C., Vaughan S., 2004, MNRAS, 347, 854
Voges W. et al., 1999, A&A, 349, 389
Williams R.J., Pogge R.W., Mathur S., 2002, AJ, 124, 3042
York D.G. et al., 2000, ApJ, 120, 1579
Zakamska N.L. et al., 2003, ApJ, 126, 2125 (Z03)
Zakamska N.L., Strauss M.A., Heckman T.M., Ivezic Z., Krolik J.H., 2004, AJ, in press (astro-ph/0406248)
Zimmermann H.U., Boese G., Becker W., Belloni T., Döbereiner S., Izzo C., Kahabka P., Schwentker O., 1998, EXSAS User's Guide, MPE Report, *ROSAT* Scientific Data Center